
Problem-orientable numerical algorithm for modelling multi-dimensional radiative MHD flows in astrophysics – the hierarchical solution scenario

Ahmad A. Hujeirat

Applied Mathematics, Universität Heidelberg, 69120 Heidelberg, Germany
ahmad.hujeirat@iwr.uni-heidelberg.de

Abstract: We present a hierarchical approach for enhancing the robustness of numerical solvers for modelling radiative MHD flows in multi-dimensions.

This approach is based on clustering the entries of the global Jacobian in a hierarchical manner that enables employing a variety of solution procedures ranging from a purely explicit time-stepping up to fully implicit schemes. A gradual coupling of the radiative MHD equation with the radiative transfer equation in higher dimensions is possible.

Using this approach, it is possible to follow the evolution of strongly time-dependent flows with low/high accuracies and with efficiency comparable to explicit methods, as well as searching quasi-stationary solutions for highly viscous flows.

In particular, it is shown that the hierarchical approach is capable of modelling the formation of jets in active galactic nuclei and reproduce the corresponding spectral energy distribution with a reasonable accuracy.

Key words: Methods: numerical – hydrodynamics – MHD – radiative transfer

1 Introduction

Within the last two decades, a tremendous progress has been made in both computational fluid dynamics (CFD) algorithms and the computer hardware technologies. The computing speed and memory capacity of computers have increased exponentially during this period. Similarly is in astrophysical fluid dynamics (AFD), which is a rapidly growing research field, and in which modern numerical methods are extensively used to model the evolution of rather complicated flows. Unlike CFD, in which implicit methods are frequently used,

the majority of the methods used in AFD are explicit. Several of them became very popular, e.g., ZEUS (ST92), NIRVANA+ (ZI98), FLASH (FR00), VAC (TO98), THARM (GA03). The popularity of explicit methods arises from their being easy to construct, vectorizable, parallelizable and even more efficient as long as dynamical evolutions of compressible flows are concerned. Specifically, for modeling the dynamical evolution of HD-flows in two and three dimensions explicit methods are highly superior to-date. For modelling relativistic flows, Koide and collaborators (KO99; KO02) and (ME01; KO99) have developed pioneering general relativistic MHD solvers. A rather complete review of numerical approaches for relativistic fluid dynamics is given in (MA99; FO00). A ZEUS-like scheme for general relativistic MHD has also been developed and is described in (VI03).

These methods, however, are numerically stable as far as the Courant-Friedrich-Levy number is smaller than unity. The corresponding time step size decreases dramatically with the incorporation of real astrophysical effects. Specifically, they may even stagnate if self-gravity, radiative and chemical effects are included. Moreover, explicit methods break down if the flow is weakly or strongly incompressible, and if the domain of calculations is subdivided into a strongly stretched mesh. In an attempt to enhance their robustness, several alternatives have been suggested, such as semi-explicit, semi-implicit or even implicit-explicit methods (KL89; TO98). Nevertheless, their rather limited range of applications has led to the fact that most of the interesting astrophysical problems remained, indeed, not really solved. A simple example is the evolution of a steady turbulent accretion disk. It was found by Balbus & Hawley (1991) that weak magnetic fields in accretion disks are amplified, generate turbulence, which in turn redistribute the angular momentum in the disk. However, whether this instability leads to the long-sought global steady accretion rate, or is it just a transient phenomenon in which the generation of turbulence is subsequently suppressed by dynamo action are not at all clear. Other notable phenomena are the formation and acceleration of the observed superluminal jets in quasars and in microquasars, the origin of the quasi-periodic oscillation in low mass X-ray binaries or the progenitors of gamma ray burst are still spectacular.

Explicit methods rely on time-extrapolation procedures for advancing the solution in time. However, in order to provide physically consistent solutions, it is necessary that these procedures are numerically stable. The usual approach for examining the stability of numerical methods is to perform the so called von Neumann analysis (see HI90, for further details). This yields the so called Courant-Friedrich-Levy condition (CFL) which is known to limit the range of application and severely affects the robustness of explicit methods. In particular, equations corresponding to physical processes occurring on much shorter time scales than the hydro-time scale (e.g., radiation, self-gravitation and chemical reactions) cannot be followed explicitly. Furthermore, these methods are not suited for searching solutions that correspond to evolutionary phases occurring on time scales much longer than the hydro-time scale. Us-

ing high performance computers to perform a large number of explicit time steps may lead to accumulation of round-off errors that can easily distort the propagation of information from the boundaries and cause divergence of the solution procedure, especially if Neumann type conditions are imposed at the boundaries. In contrast to explicit methods, implicit methods are based on

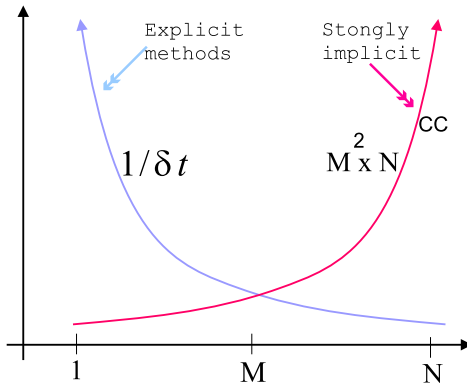


Fig. 1. A schematic description of the time step size and the computational costs versus the band width M of the Jacobian. N is the number of unknowns. Explicit methods correspond to $M = 1$ and large $1/\delta t$. They require minimum computational costs (CC). Large time steps (i.e., small $1/\delta t$) can be achieved using strongly implicit methods. These methods generally rely on the inversion of matrices with large band width, hence computationally expensive, and, in most cases, are inefficient.

solving a matrix equation of the form $Ax = b$, where A is the Jacobian matrix corresponding to the system of equations to be solved, b is the right hand side vector of known quantities, and x is the solution vector sought. These methods have two major drawbacks. First, constructing the matrix A is difficult, time consuming, and may considerably influence the robustness of the method. Second, the inversion procedure must be stable and efficient. In general, conservative discretization of the MHD equations give rise to sparse matrices, or even to narrow band matrices. Therefore, any efficient matrix inversion procedure must take the advantage of A being sparse. Inverting A directly by using Gaussian elimination requires N^3 algebraic operations, where N is the number of unknowns. If the flow is multi-dimensional and a high spatial resolution is required, the number of operations can be prohibitive even on modern supercomputers. Krylov Sub-Iterative Methods (KSIMs), on the other hand, are most suited for sparse matrices and avoid the fill-in procedure. In the latter case, A is not directly involved in the process, but rather its multiplication with a vector. The convergence rate of KSIMs has been found to depend strongly on the proper choice of the pre-conditioner. For advection-dominated

flows, incomplete factorization such as ILU, IC and LQ, approximate factorization, ADI, line Gauss-Seidel are only a small sub-set of possible sequential pre-conditioners (see SA00, and the references therein). Another powerful way of accelerating relaxation techniques is to use the multi-grid method as a direct solver or as a pre-conditioner (BR01; TR01). For parallel computations, Red-Black ordering in combination with GRMES and Bi-CGSTAB as well as domain decomposition are among the popular pre-conditioners (see DO98, for further discussion.)

Towards studying the jet-disk-BH connection in AGNs and μ -QSOs a series of multi-dimensional calculations have been performed (e.g., OU97; UC99; ME03; HUI2; HUI5; HUI6). Specifically, these studies revealed that:

1. Counter-rotating disks with respect to the BH-spin generate jets that propagate approximately twice as fast as in the co-rotating case.
2. Jets formed are found to be relatively slow, i.e., the corresponding Γ -factors did not reach the desired large values. This was found in both cases: when the spins of the disk and the BH are parallel and when they are anti-parallel. Moreover, disks surrounding Kerr BHs have been verified to produce jets that are more powerful than in the Schwarzschild case. These jets are driven primarily by strong MFs that are created by the frame dragging effect.
3. Large Γ -factors are obtainable if the Alfvén speed due to the PMF is equal to or even larger than the local escape velocity (see ME03, and the references therein).
4. Poloidal magnetic fields may extract rotational energy from the disk plasma, and from a geometrically thin super-Keplerian layer between the disk and the overlying corona. The outflowing plasma in this layer is dissipative, two-temperature, virial-hot, advective and electron-proton dominated. The innermost part of the disk in this model is turbulent-free, sub-Keplerian rotating and advective-dominated. This part ceases to radiate as a standard disk, and most of the accretion energy is converted into magnetic and kinetic energies that go into powering the jet.

Nevertheless, jet-structures, their formation, acceleration, their linkage to the accretion phenomena and the nature of their plasma are still a matter of debate. Furthermore, the flood of observational data makes it even more essential than ever to perform sophisticated numerical calculations to gain a more precise insight of their evolution.

In this paper we focus on the architecture of the global solution procedure rather than on local details, such as order of accuracies, physical consistency, types of advection schemes or fulfilling the solenoidal condition. Specifically, we discuss strategies for enhancing the robustness of solvers through constructing various pre-conditionings to implement a variety of solution methods in arbitrary dimensions. Special attention is given to radiative MHD solvers

and their possible coupling with the radiative transfer equation in higher dimensions.

2 The governing equations

2.1 The 3D axi-symmetric radiative MHD equations

Spherical geometry is the most appropriate geometry for capturing flow configurations in the vicinity of black holes. Taking into account the perfect axi-symmetry of black holes, and that their gravitational pull dominates the forces exerting on the surrounding flows, we conclude that axi-symmetry is a reasonable assumption that may characterize accretion flows in their vicinities. Moreover, in applying spherical geometry the transformation $\bar{\theta} = \pi/2 - \theta$ has been used¹. We note that the dynamical time scale near the event horizon is extremely short, therefore giving rise to multi-component flows, such as electron and ion plasmas.

In the following we describe the set of radiative MHD equations, and list the scaling variable that may be used for transforming them into non-dimensional form (see Table 1).

- Continuity equation:

$$\frac{\partial \rho}{\partial t} + \nabla \cdot \rho V = 0 \quad (1)$$

- Radial momentum equation:

$$\frac{\partial m}{\partial t} + \nabla \cdot mV = \frac{\partial P}{\partial r} + \rho \frac{(V_\theta^2 + V_\varphi^2)}{r} + \rho \frac{\partial \Phi}{\partial r} + \lambda_{\text{FLD}} \frac{\partial E}{\partial r} + F_L^r + Q_{\text{vis}}^r \quad (2)$$

- Vertical momentum equation:

$$\frac{\partial n}{\partial t} + \nabla \cdot nV = \frac{\partial P}{\partial \theta} - \rho V_\varphi^2 \tan \theta + \rho \frac{\partial \Phi}{\partial \theta} + \lambda_{\text{FLD}} \frac{\partial E}{\partial \theta} + F_L^\theta + Q_{\text{vis}}^\theta \quad (3)$$

- Angular momentum equation:

$$\frac{\partial \ell}{\partial t} + \nabla \cdot \ell V = F_L^\varphi + Q_{\text{vis}}^\varphi \quad (4)$$

- Internal equation of the ions:

$$\frac{\partial \mathcal{E}_i^{\text{d}}}{\partial t} + \nabla \cdot \mathcal{E}_i^{\text{d}} V = -(\gamma - 1) \mathcal{E}_i^{\text{d}} \nabla \cdot V + \Phi - A_{i-e} + \nabla \cdot \kappa_i^{\text{cond}} \nabla T_i \quad (5)$$

- Internal equation of the electrons:

$$\frac{\partial \mathcal{E}_e^{\text{d}}}{\partial t} + \nabla \cdot \mathcal{E}_e^{\text{d}} V = -(\gamma - 1) \mathcal{E}_e^{\text{d}} \nabla \cdot V + A_{i-e} - A_B - A_C - A_{\text{Syn}} + \nabla \cdot \kappa_e^{\text{cond}} \nabla T_e \quad (6)$$

¹This transformation allows simple analogy with and into cylindrical coordinates.

- Equation of the zero moment of the radiation field:

$$\frac{\partial E}{\partial t} + \nabla \cdot EV + \nabla \cdot [\lambda_{\text{FLD}} \nabla E] - \Lambda_B + \Lambda_C + \Lambda_{\text{Syn}} \quad (7)$$

- The induction equation:

$$\frac{\partial B}{\partial t} = \nabla \times (V \times B + \alpha_{\text{dyn}} B - \nu_{\text{mag}} \nabla \times B). \quad (8)$$

- Gravitational potential: the Poisson equation:

$$\Delta \psi = 4\pi G \rho, \quad (9)$$

where ψ is the gravitational potential and G is the gravitational constant.

In Table (2) we list part of the variables used and their definitions. Further,

Scaling variables:

Mass:	$\tilde{\mathcal{M}} = 3 \times 10^8 M_\odot$
Accretion rate:	$\tilde{\dot{\mathcal{M}}} = 10^{-1} \dot{\mathcal{M}}_{Edd}$
Distance:	$\tilde{R} = R_{\text{in}} = 3R_S$, where $R_S = 2G\tilde{\mathcal{M}}/c^2$
Temperature:	$\tilde{T} = 5 \times 10^7 K$
Velocities:	$\tilde{V} = \tilde{V}_S = [\gamma \mathcal{R}_{\text{gas}} \tilde{T} / \mu_i]^{1/2}$, $\mu_i = 1.23$
Ang. Velocity:	$\tilde{V}_\varphi = \tilde{V}_{\text{Kep}} = (G\tilde{\mathcal{M}}/\tilde{R})^{1/2}$
Magnetic Fields:	$\tilde{B} = \tilde{V}_S / \sqrt{4\pi \tilde{\rho}}$
Density:	$\tilde{\rho} = \tilde{\dot{\mathcal{M}}} / (\tilde{H}_d \tilde{R}_{\text{out}} \tilde{V}_S) = 2.5 \times 10^{-12} g cm^{-3}$

Table 1. Scaling variables for reformulating the MHD equations in non-dimensions.

the subscripts “i” and “e” correspond to ion and electron plasmas, where $\gamma = 5/3$, $\mu_i = 1.23$ and $\mu_e = 1.14$ are used. α_{dyn} , η_{mag} correspond to the α -dynamo and the magnetic diffusivity, respectively. The radiative diffusion coefficient λ_{FLD} is a radiative flux limiter which forces the radiative flux to adopt the correct form in optically thin and thick regions, i.e.,

$$\nabla \cdot \lambda_{\text{FLD}} \nabla E = \begin{cases} \nabla \cdot \frac{1}{3\chi} \nabla E & \text{if } \tau \gg 1 \\ \nabla \cdot nE & \text{if } \tau \ll 1, \end{cases} \quad (10)$$

and provides a smooth matching in the transition regions. Here $\chi = \rho(\kappa_{\text{abs}} + \sigma)$ and $n = \nabla E / |\nabla E|$, where κ_{abs} and σ are the absorption and scattering coefficients. Λ_B , Λ_{i-e} , Λ_C , Λ_{Syn} correspond to Bremsstrahlung cooling, Coulomb coupling between the ions and electrons, Compton and synchrotron coolings, respectively (RY79). These processes read:

$$\begin{aligned} \Lambda_{i-e} &= 5.94 \times 10^{-3} n_i n_e c k \frac{(T_i - T_e)}{T_e^{3/2}} / \mathcal{N} \\ \Lambda_B &= 4ac\kappa_{\text{abs}} \rho (T^4 - E) / \mathcal{N}, \\ \Lambda_C &= 4\sigma n_e c \left(\frac{k}{m_e c^2} \right) (T_e - T_{\text{rad}}) E / \mathcal{N}, \end{aligned} \quad (11)$$

where $\mathcal{N} = [(\gamma - 1)/\gamma](\tilde{V}^2\tilde{V}_\varphi/\tilde{R})$ is a normalization quantity. n_e , n_i are the electron- and ion-number densities. E is the density of the radiative energy, i.e., the zero-moment of the radiative field. The radiative temperature is defined as $T_{rad} = E^{1/4}$. The Lorenz forces acting on charged plasma in the MHD approximation read:

$$\begin{aligned} F_L^r &= \frac{B_\theta}{r} \frac{\partial B_r}{\partial \theta} - \frac{1}{r} \frac{\partial}{\partial r} r (B_\theta^2 + B_T^2) + \frac{1}{2} \frac{\partial}{\partial r} (B_\theta^2 + B_T^2) \\ F_L^\theta &= B_r \frac{\partial}{\partial r} r B_\theta - \frac{1}{2} \frac{\partial}{\partial \theta} B_r^2 - \left[\frac{1}{\cos \theta} \frac{\partial}{\partial \theta} \cos \theta B_T^2 - \frac{1}{2} \frac{\partial}{\partial \theta} B_T^2 \right] \\ F_L^\varphi &= B_p \cdot \nabla \bar{B} = B_r \frac{\partial}{\partial r} (r \cos \theta B_T) + \frac{B_\theta}{r} \frac{\partial}{\partial \theta} (r \cos \theta B_T). \end{aligned} \quad (12)$$

The turbulent-diffusive terms read:

$$\begin{aligned} Q_{vis}^r &= \frac{1}{r^2} \frac{\partial}{\partial r} (r^2 T_{rr}) + \frac{1}{r \cos \theta} \frac{\partial}{\partial \theta} (\cos \theta T_{r\theta}) + \frac{T_{rr}}{r} \\ Q_{vis}^\theta &= \frac{1}{r^2} \frac{\partial}{\partial r} (r^2 T_{r\theta}) + \frac{1}{r \cos \theta} \frac{\partial}{\partial \theta} (\cos \theta T_{\theta\theta}) + T_{\phi\phi} \tan \theta \\ Q_{vis}^\phi &= \frac{1}{r^2} \frac{\partial}{\partial r} (r^2 T_{r\phi}) + \frac{1}{r \cos \theta} \frac{\partial}{\partial \theta} (r \cos^2 \theta T_{\theta\phi}), \end{aligned} \quad (13)$$

where

$$\begin{aligned} T_{rr} &= 2\eta \left(\frac{\partial V_r}{\partial r} - \frac{1}{3} \left(\frac{1}{r^2} \frac{\partial r^2 V_r}{\partial r} + \frac{1}{r \cos \theta} \frac{\partial}{\partial \theta} (\cos \theta V_\theta) \right) \right) \\ T_{\theta\theta} &= 2\eta \left(\frac{1}{r} \frac{\partial V_\theta}{\partial \theta} + \frac{V_r}{r} - \frac{1}{3} \left(\frac{1}{r^2} \frac{\partial r^2 V_r}{\partial r} + \frac{1}{r \cos \theta} \frac{\partial}{\partial \theta} (\cos \theta V_\theta) \right) \right) \\ T_{\phi\phi} &= 2\eta \left(\frac{V_\theta}{r} \tan \theta + \frac{V_r}{r} - \frac{1}{3} \left(\frac{1}{r^2} \frac{\partial r^2 V_r}{\partial r} + \frac{1}{r \cos \theta} \frac{\partial}{\partial \theta} (\cos \theta V_\theta) \right) \right) \\ T_{\theta\phi} &= \eta \frac{\cos \theta}{r} \frac{\partial}{\partial \theta} \left(\frac{V_\varphi}{\cos \theta} \right) \\ T_{r\phi} &= \eta r \frac{\partial}{\partial r} \left(\frac{V_\varphi}{r} \right) \\ T_{r\theta} &= \eta \left(r \frac{\partial}{\partial r} \left(\frac{V_\theta}{r} \right) + \frac{1}{r} \frac{\partial V_r}{\partial \theta} \right). \end{aligned} \quad (14)$$

2.2 The isotropic radiation transfer equation: The Kompaneets equation

Compton up-scattering of soft photons is most efficient in unsaturated Comptonization regions where the Compton-Y parameter is of order unity. This parameter acquires large values in optically thick media, and small values in the corona, implying that the corona-disk interaction region and/or the innermost region of the disk are most appropriate for this process to operate efficiently. As a consequence, Comptonization in accretion flows is intrinsically two-dimensional, and therefore requires a multi-dimensional treatment. So far, Comptonization has been considered under strong assumptions

Symbols:

\mathbf{V}	$= (V_r, V_\theta, V_\varphi)$	velocity field
\mathbf{B}	$= (B_r, B_\theta, B_\Gamma) = (B_p, B_\Gamma)$	magnetic field
∇	$= \left(\frac{\partial}{\partial r}, \frac{1}{r} \frac{\partial}{\partial \theta} \right)$	gradient in spherical coordinates
$\nabla \cdot$	$= \frac{1}{r^2} \frac{\partial}{\partial r} r^2 + \frac{1}{r \cos \theta} \frac{\partial}{\partial \theta} \cos \theta$	divergence in spherical coordinates
$T^{e,i}$	$=$	electron and ion temperatures
$P^{e,i}$	$= \mathcal{R}_{\text{gas}} \rho (T_i / \mu_i + T_e / \mu_e)$	electron and ion pressure
$\mathcal{E}^{e,i}$	$= P^{e,i} / (\gamma - 1),$	electron and ion internal energies
$\kappa^{e,i}$	$= 7.8 \times T_e^{3/2}, 3.2 \times T_i^{3/2}$	electron and ion conductivities
(m, n, ℓ)	$= \rho (V_r, r V_\theta, r \cos \theta V_\varphi)$	momentum
$\nu (= \eta / \rho), \nu_{\text{mag}}$	$=$	turbulent and magnetic diffusivities
Φ	$= \Phi_{\text{HD}} + \Phi_{\text{MHD}}$	HD and MHD turbulent dissipation (see MM).

Table 2. Variables used and their definitions

that allow separation of variables and lead to the separation of the Kompaneets operator from the radiative transfer equation. Here, the radiative intensity is assumed to be time-independent, isotropic and the plasma is isothermal. In this case, the generation and Comptonization of photons can be described by a second order differential equation in the frequency space (IL72; FE72; KA76; SH76; HUIJ3).

Different accretion models display different spectra. Therefore, it is essential to perform a diagnostic study to analyze their consistency with observations. This however requires solving the 7D radiation transfer equation:

$$\frac{1}{c} \frac{\partial I}{\partial t} + n \cdot \nabla I = \kappa_\nu \rho (S_\nu - I) - \sigma \rho I + \int CI d\hat{\Omega} d\hat{E} + \varepsilon_\nu^{\text{mod}}, \quad (15)$$

where $I = I(t, r, \theta, \varphi, \vartheta, \phi, \nu)$ is the radiative intensity which depends on time t , the spherical coordinates (r, θ, φ) , two ordinates (ϑ, ϕ) that determine the direction of the photons on the unit sphere, and on the frequency ν . κ_ν and σ are the absorption and scattering coefficients. S_ν is a source function. $I_{\text{int}} \doteq \int CI d\hat{\Omega} d\hat{E}$ describes the scattering of photons through electrons, and C is the scattering kernel. $\varepsilon_\nu^{\text{mod}}$ is the modified synchrotron emission.

To make the problem tractable, the following approximations have been performed:

- The radiation field is axi-symmetric and isotropic, i.e., $\partial/\partial\varphi = 0$ and $J = \frac{1}{2\pi} \int I d\hat{\Omega} \approx I$.
- The source function is represented by the modified black body function, i.e.,

$$S_\nu = B_\nu^{\text{mod}} = \frac{2B_\nu}{1 + \sqrt{1 + \frac{\sigma}{\kappa_\nu}}}, \quad (16)$$

where B_ν is the normal Planck function (see RY79).

- The thermal energy of the electrons is far below its corresponding rest mass energy, i.e., $\epsilon = \frac{kT}{m_e c^2} \ll 1$, and $\frac{h\nu}{m_e c^2} \ll 1$.

Using the last approximation, I_{int} can be expanded up to second order in ϵ which reduces it to the so-called Kompaneets operator (PA80):

$$I_{\text{int}} \Leftrightarrow \mathcal{K}_\nu = -\frac{\nu}{m_e c^2} \frac{\partial}{\partial \nu} (4kT - h\nu)I + \frac{kT\nu}{m_e c^2} \frac{d^2}{d\nu^2} (\nu I). \quad (17)$$

In this case, the radiative transfer equation with respect to a rest frame of reference reads:

$$\begin{aligned} \frac{1}{c} \left[\frac{\partial E_\nu}{\partial t} + \nabla \cdot V E_\nu \right] = & -\lambda_\nu (\nabla \cdot V) E_\nu + \nabla \cdot \left[\frac{\lambda_\nu}{\chi_\nu} \nabla E_\nu \right] \\ & + \kappa_\nu \rho (S_\nu - E_\nu) + \mathcal{K}_\nu + \varepsilon_\nu^{\text{mod}}, \end{aligned} \quad (18)$$

where $E_\nu = \frac{4\pi}{c} J = E(t, r, \theta, \nu)$, $\chi_\nu = \rho(\kappa_\nu + \sigma)$, λ_ν is the flux limited diffusion coefficient (LE81), which forces the radiative flux to adopt the correct form in optically thin and thick regions, i.e.,

$$\nabla \cdot [\lambda_\nu \nabla E_\nu] = \begin{cases} \nabla \cdot \left[\frac{1}{3\chi_\nu} \nabla E_\nu \right] & \text{if } \tau \gg 1 \\ \nabla \cdot n E_\nu & \text{if } \tau \ll 1. \end{cases} \quad (19)$$

λ_ν may provide a smooth matching between these two extreme regimes. The above two different behaviour of the operator can be combined as follows:

$$\nabla \cdot \lambda_\nu \nabla_\nu E_\nu \hookrightarrow \nabla \cdot \eta_r \nabla E_\nu, \quad (20)$$

where $\eta_r = (1 - \alpha) \frac{\nabla E_\nu}{|\nabla E_\nu|} + \alpha \frac{1}{3\chi}$, $\alpha = e^{-R_{\text{FLD}}}$, and $R_{\text{FLD}} = \nabla E / \rho(\kappa_\nu S_\nu + \sigma E_\nu)$ (HUJ0).

$\varepsilon_\nu^{\text{mod}}$ in Eq. (15) corresponds to the modified synchrotron emission of photons by relativistic electrons gyrating around magnetic field lines, which reads:

$$\varepsilon_\nu^{\text{mod}} = \xi \varepsilon_\nu + (1 - \xi) \varepsilon_\nu^{\text{BB}},$$

where $\xi (\doteq e^{-(\nu_c/\nu)^2})$ is a switch on/off operator which bridges optically thin and thick media to synchrotron radiation, and ν_c is a critical frequency (see below).

An appropriate approximation for ε_ν in optically thin medium reads (MA96):

$$\varepsilon_\nu = 2.73 \times 10^{-5} \frac{\rho \nu}{K_2(1/\theta_e)} \tilde{\mathcal{I}}(\nu, B, \Theta) \text{ ergs cm}^{-3} \text{ s}^{-1} \text{ Hz}^{-1}, \quad (21)$$

where K_2 is the Bessel function of the second kind and $\tilde{\mathcal{I}} = \frac{4.05}{\zeta^{1/6}} (1 + \frac{0.4}{\zeta^{1/4}} + \frac{0.53}{\zeta^{1/2}}) e^{-1.89\zeta^{1/3}}$.

Here $\zeta = 2.38 \times 10^{-7} (\nu/B\theta_e^2)$ and $\theta_e = kT_e/m_e c^2$.

Below a certain critical frequency ν_c , the media become self-absorbing to synchrotron emission. In this case, $\varepsilon_\nu^{\text{mod}} \approx \varepsilon_\nu^{\text{BB}} = 2\pi \frac{\nu^2}{c^2} kT$. To find ν_c , we use the local non-linear Newton iteration procedure applied to the equation

$$\int_V \varepsilon_\nu dV = \int_S \varepsilon_\nu^{\text{BB}} dS. \quad (22)$$

Having obtained ν_c , the switch on/off operator ξ can then be constructed.

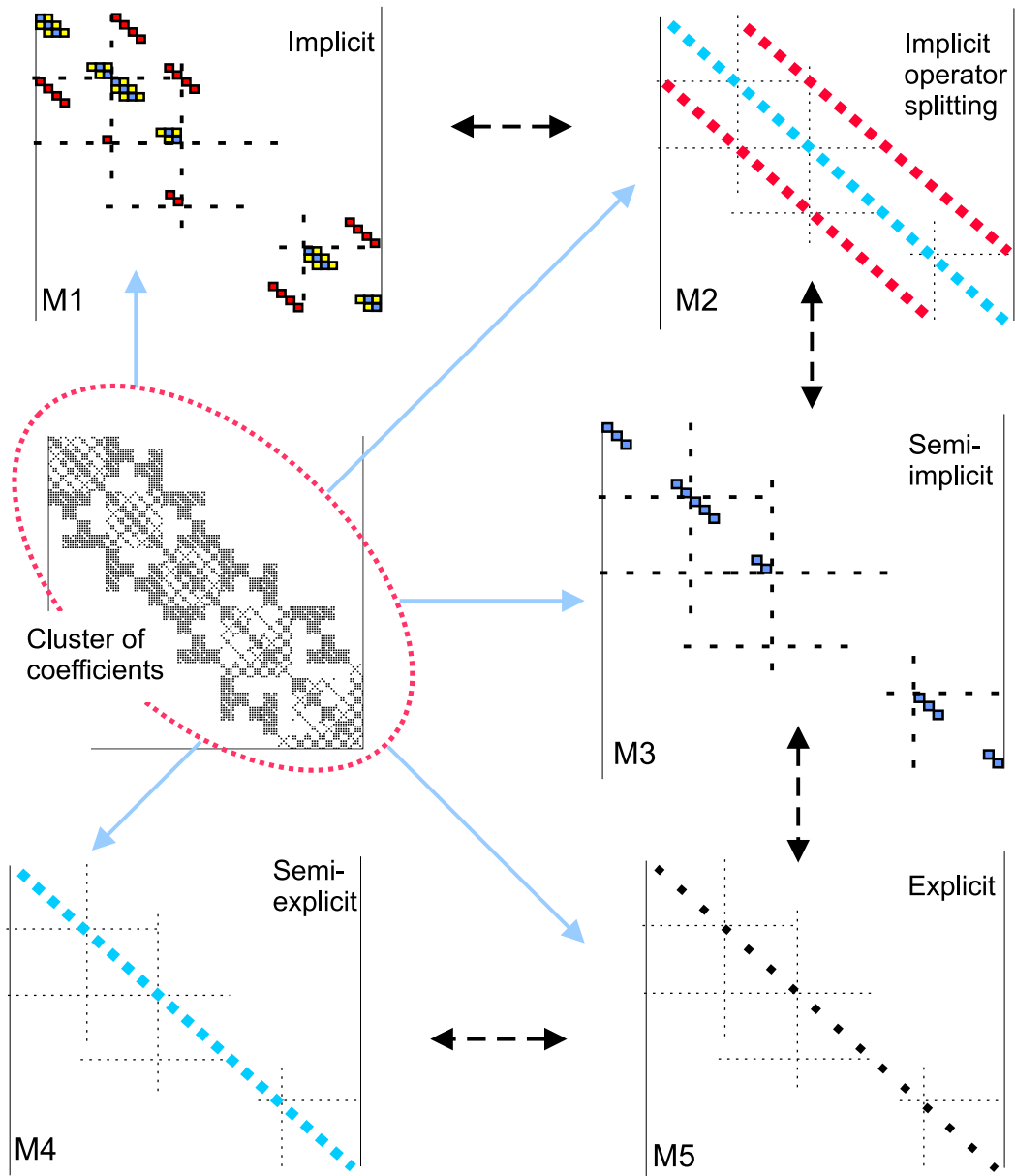


Fig. 2. A schematic description of the hierarchical solution method. A cluster of coefficients is computed in the first stage, and a matrix-generator is created that allows using various solution procedures ranging from purely explicit to fully implicit. Interchange between solution methods is possible, as modifying, adding or removing entries is directly maintainable.

3 Solution methods

3.1 Solving the radiative MHD equations

The set of equations in conservative form may be written in the following vector form:

$$\frac{\partial \mathbf{q}}{\partial t} + L_{r,rr} \mathbf{F} + L_{\theta,\theta\theta} \mathbf{G} = \mathbf{f}, \quad (23)$$

where F and G are fluxes of q , and $L_{r,rr}$, $L_{\theta,\theta\theta}$ are first and second order transport operators that describe advection-diffusion of the vector variables \mathbf{q} in r and θ directions. \mathbf{f} corresponds to the vector of source functions.

Adopting a five star staggered grid discretization, it is easy to verify that at each grid point the Eq. (23) acquires the following block matrix equation:

$$\begin{aligned} \frac{\delta q_{j,k}}{\delta t} + \underline{S}^r \delta q_{j-1,k} + D^r \delta q_{j,k} + \overline{S}^r \delta q_{j+1,k} \\ + \underline{S}^\theta \delta q_{j,k-1} + D^\theta \delta q_{j,k} + \overline{S}^\theta \delta q_{j,k+1} = RHS_{j,k}^n, \end{aligned} \quad (24)$$

where the subscripts “j” and “k” denote the grid-numbering in the r and θ directions, respectively, and $RHS^n = [\mathbf{f} - L_{r,rr} \mathbf{F} - L_{\theta,\theta\theta} \mathbf{G}]^n$. Underlines (overlines) mark the sub-diagonal (super-diagonal) block matrices in the corresponding directions, and $D^{r,\theta}$ are the diagonal block matrices.

To outline the directional dependence of the block matrices, we re-write Eq. 24 in a more compact form:

$$\begin{aligned} \overline{S}^\theta \delta q_{j,k+1} \\ + \underline{S}^r \delta q_{j-1,k} + D_{\text{mod}} \delta q_{j,k} + \overline{S}^r \delta q_{j+1,k} = RHS_{j,k}^n \\ + \underline{S}^\theta \delta q_{j,k-1}, \end{aligned} \quad (25)$$

where $D_{\text{mod}} = \delta q_{j,k}/\delta t + D^x + D^y$. Eq. (25) gives rise to at least four different types of solution procedures:

1. Classical explicit methods are very special cases in which the sub- and super-diagonal block matrices together with D^x and D^y are neglected. The only matrix to be retained here is $(1/\delta t) \times$ (the identity matrix), i.e., the first term on the LHS of Eq. 24. This yields the vector equation (see M5/Fig. 2):

$$\left[\frac{I}{\delta t}\right] \delta q_{j,k} = RHS_{j,k}^n. \quad (26)$$

2. Semi-explicit methods are obtained by preserving the diagonal entries, $d_{j,k}$, of the block diagonal matrix D_{mod} (see M4/Fig. 2). This method has been verified to be numerically stable even when large Courant-Friedrich-Levy (CFL) numbers are used. In particular, this method is absolutely stable if the flow is viscous-dominated.

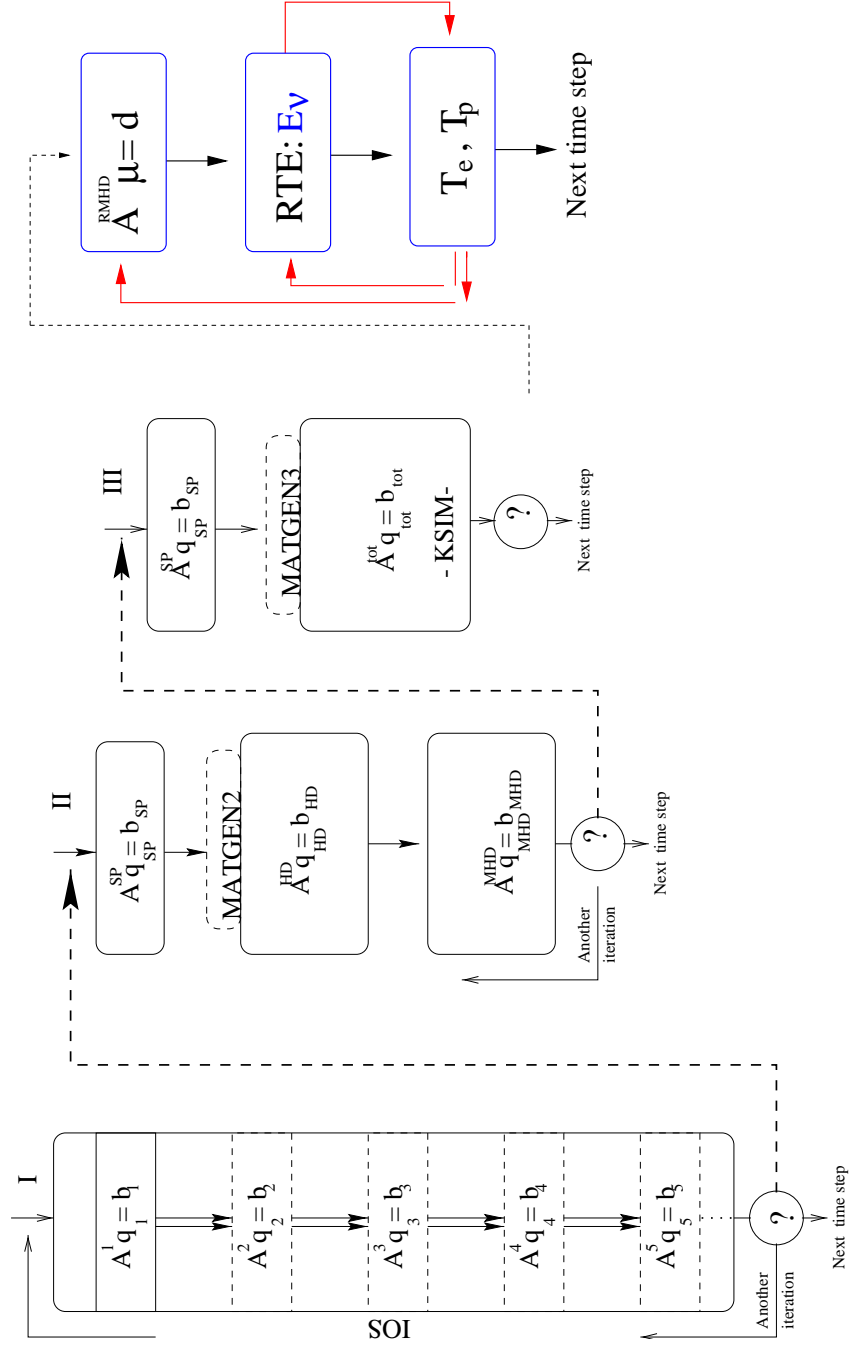


Fig. 3. A schematic description of the hierarchical algorithm for solving the radiative MHD equations. Stage I corresponds to the implicit operator splitting approach (IOS), which is most appropriate for following the early time-dependent phases of the flow. The solution obtained can then be used as initial condition for Stage II, where the hydro-equations are solved as a single coupled system, followed by the magneto component, which is again solved as a single coupled system. Here, high spatial and temporal accuracies in combination with the prolongation/restriction strategy may be used. Similarly, the solution obtained in this stage may be used as starting solutions for Stage III, where steady solutions for the fully coupled set of equations consisting of the zero moment of the radiation field and the MHD equations are sought. In this stage, pre-conditioned Krylov sub-iterative methods are considered to be robust and efficient. The very last stage, Stage IV, corresponds to the case where solutions for the internal energy equations weakly coupled with the 5D radiative transfer equation are sought.

3. Semi-implicit methods are recovered when neglecting the sub- and super-diagonal block matrices only, but retaining the block diagonal matrices (see M3/Fig. 2). In this case the matrix equation reads:

$$D_{\text{mod}}\delta q_{j,k} = R H S_{j,k}^n. \quad (27)$$

We note that inverting D_{mod} is a straightforward procedure, which can be maintained analytically or numerically.

4. A fully implicit solution procedure requires retaining all the block matrices on the LHS of Eq. 25. This yields a global matrix that is highly sparse (M1/Fig.2). In this case, the ‘‘Approximate Factorization Method’’ (-AFM: BW78) and the ‘‘Line Gauss-Seidel Relaxation Method’’ (-LGS: MA85) are considered to be efficient preconditionings for the set of radiative MHD-equations.

In the case that only stationary solutions are sought, convergence to steady state can be accelerated by adopting the so called the ‘‘Residual Smoothing Method’’ (see HJ8, and the references therein).

This method is based on associating a time step size with the local CFL-number at each grid point. While this strategy is efficient at providing quasi-stationary solutions within a reasonable number of iterations, it is incapable at providing physically meaningful time scales for features that possess quasi-stationary behaviour. Here we suggest to use the obtained quasi-stationary solutions as initial configuration and re-start the calculations using a uniform and physically relevant time steps.

3.2 The 5D axi-symmetric RT equation: method of solution

Let $\mathcal{L}E = 0$ be the equivalent operator form of Equation 18 in the continuous space Ω_C . $\mathcal{L}E$ consists of several terms, each of which requires a careful and different representation in the finite discretization space Ω_h which is defined as $[t_1, t_2, \dots, t_N] \otimes [r_1, r_2, \dots, r_J] \otimes [\theta_1, \theta_2, \dots, \theta_K] \otimes [\nu_1, \nu_2, \dots, \nu_M]$. $[t]$, $[r]$, $[\theta]$ and $[\nu]$ correspond to time, radius (spherical), latitude, and to the frequency intervals, respectively.

In most astrophysical problems, radiative effects occur on relatively short time scales compared to the hydro- or magneto-hydrodynamical ones, for which the use of unconditionally implicit numerical solvers is essential. This requires however that all terms of Eq. (18) should be evaluated on the new time-level. The discretization used should assure that the resulting Jacobian $A_{r\theta\nu} = \partial\mathcal{L}E/\partial E$ is diagonally dominant. Therefore, the following procedures are employed.

- The advection term $\nabla \cdot V E_\nu$ is discretized using a second order up-winding.

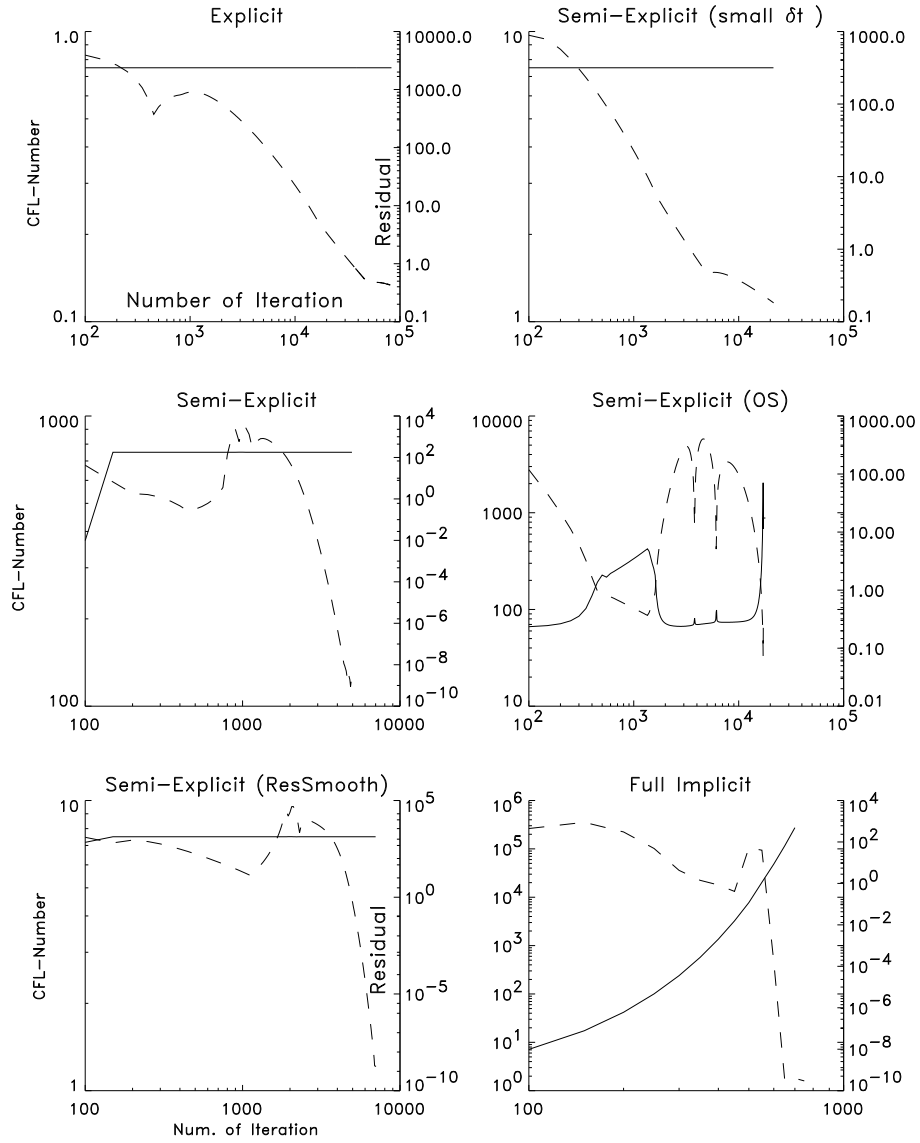


Fig. 4. The problem of free-fall of gas onto a Schwarzschild black hole. The evolution of the CFL-number and the residual versus number of iterations are shown, using different solution procedures. The solution methods are: normal explicit (top/left), semi-explicit (middle/left), semi-explicit in combination with the residual smoothing strategy (bottom/left), semi-explicit using moderate CFL-numbers (top/right), semi-explicit method in which the time step size is taken to be a function of the maximum residual (middle/right), and finally the fully implicit method (bottom/right). The different forms of the semi-explicit method used here are stable and converges to the stationary solution, though at remarkably different rates.

Fig. 5. Free-fall of gas onto a black hole surrounded by a static cold disk. Top: the density distribution (red: large values, blue: low values, green: intermediate values). Middle: the temperature distribution (red: large values, blue: low values, gray: intermediate values). The curved shock front, where the temperature attains maxima is obvious. Bottom: the distribution of the velocity field is shown.

- The second order diffusion term $\nabla \cdot [\lambda_\nu \nabla E_\nu]$ is discretized using second order central-difference scheme on a staggered grid
- \mathcal{K}_ν contains advection and diffusion terms in the frequency space. Here up-winding discretization in the frequency space is used.

Combining the contributions of all terms of Eq. (18), we obtain at each grid point the following equation:

$$\begin{aligned} & \underline{S}^r E_{j-1,k,m}^{\text{new}} + \overline{S}^r E_{j+1,k,m}^{\text{new}} + \underline{S}^\theta E_{j,k-1,m}^{\text{new}} \\ & + \overline{S}^\theta E_{j,k+1,m}^{\text{new}} + \underline{S}^\nu E_{j,k,m-1}^{\text{new}} + \overline{S}^\nu E_{j,k,m+1}^{\text{new}} \\ & + (D^r + D^\theta + D^\nu) E_{j,k,m}^{\text{new}} = RHS, \end{aligned} \quad (28)$$

where $\underline{S}^r = \partial \mathcal{L} E_\nu / \partial E_{j-1,k,m}$, $\overline{S}^r = \partial \mathcal{L} E_\nu / \partial E_{j+1,k,m}$, $D^r + D^\theta + D^\nu = \partial \mathcal{L} E_\nu / \partial E_{j,k,m}$, $\underline{S}^\theta = \partial \mathcal{L} E_\nu / \partial E_{j,k-1,m}$, $\overline{S}^\theta = \partial \mathcal{L} E_\nu / \partial E_{j,k+1,m}$, $\overline{S}^\nu = \partial \mathcal{L} E_\nu / \partial E_{j,k,m+1}$ and $\underline{S}^\nu = \partial \mathcal{L} E_\nu / \partial E_{j,k,m-1}$. The terms \underline{S}^r , D^r , and \overline{S}^r correspond to the sub-diagonal, diagonal and super-diagonal entries of the Jacobian $A_{r\theta\nu}$ in the radial direction respectively. A similar description applies to the θ - and ν -directions.

Thus, solving the equation at all grid points, is equivalent to solve matrix equation: $A_{r\theta\nu} E^{\text{new}} = E^{\text{old}}$, or simply, $Aq = b$.

This matrix is highly sparse, and pre-conditionings such as the Alternating Direction Implicit (ADI) and the Approximate Factorization Methods (AFM) are considered to be efficient. However, ADI is not appropriate for searching steady solution in three or more dimensions, as it is numerically unstable in high dimensions (FL88). Alternatively, we have tried the AFM as a pre-conditioner. However, it turns out that the AFM converges slower than our favorite iterative method: ‘Black-White-Brown’ line Gauss-Seidel method (henceforth BWB-LGS, see HI90, for further details). The latter method preserves the diagonal dominance of A , and hence converges faster than AFM. It should be noted that the line Gauss-Seidel method in its classical form is not appropriate for vector and parallel machines, mainly because the vector-length is proportional to the number of unknowns in one direction. A reasonable way to extend the vector-length is to solve for all unknowns located on even-numbered grid points, and subsequently on odd-numbered grid points. The resulting vector-length in this case is proportional to the number of unknowns in the plane under consideration, and therefore enabling enhancement efficiency when using vector or parallel machines.

More specifically, in each plane we perform two sweeps: in the first sweep we consider the unknowns in the $r - \theta$ plane, i.e., we solve the system of equations:

$$\underline{S}^r \delta E_{j-1,k,m}^{\text{new}} + (D^r + D^\theta + D^\nu) \delta E_{j,k,m}^{\text{new}} + \overline{S}^r \delta E_{j+1,k,m}^{\text{new}} = RHS,$$

where $j = 1 \rightarrow J$ and k runs over odd-numbered rows. In the second sweep, we solve:

$$\begin{aligned} \underline{S}^r \delta E_{j-1,k,m}^{\text{new}} + (D^r + D^\theta + D^\nu) \delta E_{j,k,m}^{\text{new}} + \overline{S}^r \delta E_{j+1,k,m}^{\text{new}} \\ = RHS + \underline{S}^\theta \delta E_{j,k-1,m}^{\text{new}} + \overline{S}^\theta \delta E_{j,k+1,m}^{\text{new}}, \end{aligned}$$

where $j = 1 \rightarrow J$ and k here runs over even-numbered rows. Therefore, we actually perform 6-inversion procedures per each time step. Here the 3-dimensional problem is replaced by three one-dimensional problems that are solved iteratively to recover the solution of the original problem. The method is relatively efficient, as the overall number of arithmetic operations scales linearly with the number of grid points ($\sim 6 \times 9 \times N$).

Fig. 6. The distribution of the Bernoulli number of accretion flows around a supermassive black hole. The Bernoulli number characterizes the energies of the flow in different regions. Gravitationally bound flows have negative total energy, whereas flows of positive total energy are gravitationally unbound, and potentially should expand to infinity. In this figure, the decrease of the Bernoulli number from large to low positive values is represented by yellow, green and red colours, whereas the blue colour corresponds to negative values. Obviously, gravitationally unbound blobs are formed in the vicinity of the black hole, which thereafter collimate under the action of magnetic fields to form the observed highly collimated jets.

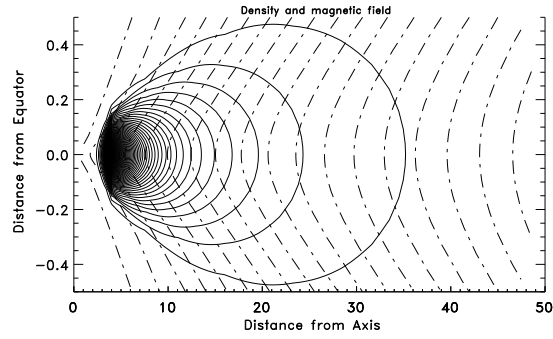


Fig. 7. The initial distribution of the density in an accretion disk ($\dot{\mathcal{M}} = 0.1 \dot{\mathcal{M}}_{\text{Edd}}$) around a Schwarzschild black hole overlaid by coronal plasmas (solid lines). The dashed lines correspond to the magnetic field lines threading the disk and the corona. The distance is given in units of $2.75 R_{\text{Sch}}$, where R_{Sch} is the Schwarzschild radius.

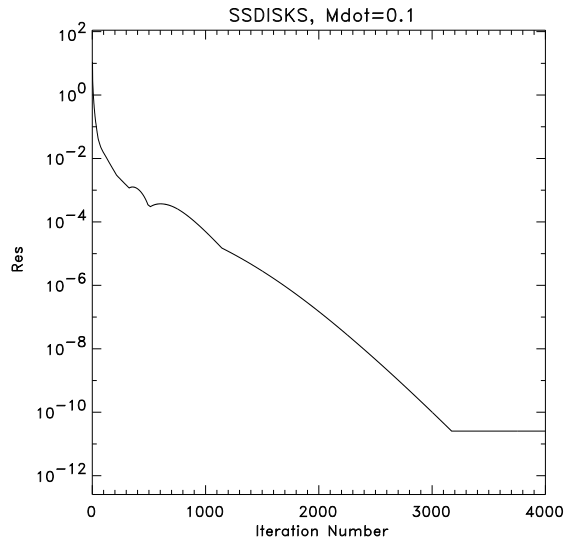


Fig. 8. The evolution of the residual in the maximum norm versus the number of iteration. The adopted density and temperature profiles correspond to standard accretion disks (see Fig. 7).

4 Validation and preliminary tests

4.1 Free-fall of plasma onto a Schwarzschild black hole

A centrifugally-unsupported gas around a spinless black hole is gravitationally bound, and therefore should fall-freely onto the black hole, provided that no

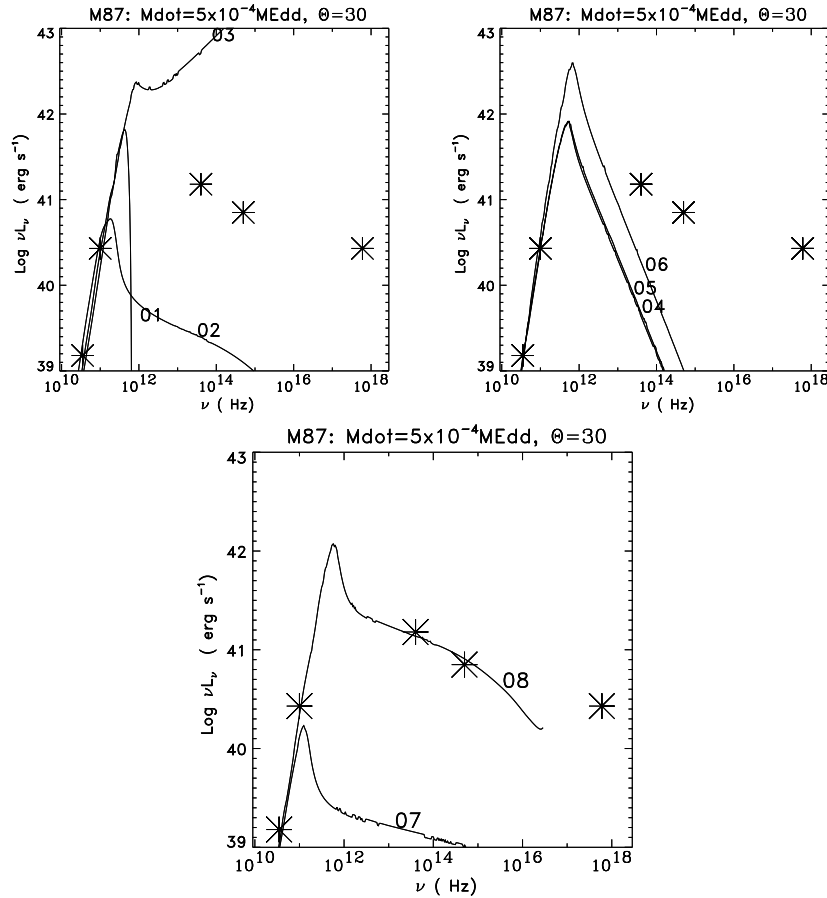


Fig. 9. A VLA image shows the active central engine of the giant elliptical galaxy M87 (top), and a NRAO radio image of the jet apparently emanating from within 100 gravitational radii. Solid lines correspond to calculated profiles and the asterisks to observational data. The profiles 01 to 06 show the spectral energy distribution calculated using different magnetic field strengths, or different truncation radii, or high/low corona temperatures. In particular, the profile 07 corresponds to a model in which the toroidal magnetic field is set to vanish artificially, whereas the poloidal magnetic field is set to be in equipartition with the thermal energy of the electrons in the transition layer between the disk and the overlying corona. The profile 08 is similar to 07, except that the toroidal magnetic field is allowed to develop and reach values beyond equipartition with respect to the thermal energy of the electrons in the transition layer between the disk and the overlying corona. The above spectral energy distribution has been obtained by solving the radiative transfer equation in 5-dimensions, taking into account the Kompaneets operator for consistently modelling Comptonization. 400 non-linearly distributed frequency points have been used to cover the frequency-space, and 125×40 finite volume cells to cover the spatial domain of the calculation.

other external forces oppose gravity. In this case, the radial distributions of the density and velocity far from the event horizon obey the power laws: $r^{-3/2}$ and $r^{-1/2}$, respectively.

This physical problem is relevant for testing the flexibility of the hierarchical scenario at adopting various solution methods, and to test their capability to capture steady, oscillation-free and advection-dominated flows, even when a strongly stretched mesh distribution is used.

The equations to be solved in this problem are the continuity, the radial and horizontal momentum equations, and the internal energy equation. The flow is assumed to be inviscid and adiabatic ($\gamma = 5/3$). The equations have been solved using a first order accurate advection scheme both in space and time. In carrying out these calculations, the following conditions/inputs have been taken into account:

- The central object is a one solar-mass and non-rotating black hole.
- The outer boundary is 100 times larger than the inner radius, i.e., $R_{\text{out}} = 100 \times R_{\text{in}}$, where R_{in} is taken to be the radius of the last stable orbit² R_{LS} . To first order in V/c , the flow at this radius can be still treated as non-relativistic, though the error can be as large as 30%.
- Along the outer boundary, the density and temperature of the gas assume uniform distributions, and flow across this boundary with the free-fall velocity. Symmetry boundary conditions along the equator, and asymmetry boundary conditions along the axis of rotation have been imposed. Along the inner boundary, we have imposed non-reflecting and outflow conditions. This means that up-stream conditions are imposed, which forbid information exterior to the boundary to penetrate into the domain of calculations. In particular, the actual values of the density, temperature and momentum in the ghost zone r are erased and replaced by the corresponding values in the last zone, i.e, the zone between R_{in} and $R_{\text{in}} + \Delta R$. In the case that second order viscous operators are considered, care has been taken to assure that their first order derivatives across R_{in} are vanished.

The above set of equations are solved in the first quadrant $[1 \leq r \leq 100] \times [0 \leq \theta \leq \pi/2]$, where 200 strongly stretched finite volume cells in the radial direction and 60 in the horizontal direction are used.

In Fig. 4, we show the evolutions of the CFL-number and the residual as function of the number of iteration which has been obtained using various numerical approaches. The results show that the convergence of the explicit and semi-explicit methods are rather slow when a relatively small time step size is used. This implies that the amplitude-limited oscillations are strongly time-dependent that may result from geometric compression. Indeed, these perturbations disappear, when relatively large time-step sizes are used (see Fig. 4, bottom/right).

² $R_{\text{LS}} = 3 \times R_{\text{S}} = 6 \times R_{\text{g}}$, where R_{S} and R_{g} are the Schwarzschild and gravitational radii, respectively.

In addition, the semi-explicit solver has been tested in combination with the residual smoothing strategy. As expected, this approach accelerates the convergence considerably (Fig. 4: compare the plots bottom/left with the top/right).

In most of the cases considered here, the time-step size is set to increase in a well-prescribed manner and independent of the residual. However, determining the size of the time step from the residual directly did not provide satisfactory convergence histories (Fig. 4, middle/right).

The results obtained here indicate that the semi-explicit method is stable and can be applied to search for stationary solutions using large time steps, or equivalently, CFL-numbers that are significantly larger than unity (Fig. 4, middle/left).

4.2 Shock formation around black holes

Similar to the forward facing step in CFD, a cold and dense disk has been placed in the innermost equatorial region: $[1 \leq r \leq 10] \times [-0.3 \leq \theta \leq 0.3]$. We use the same parameters, initial and boundary condition as in the previous flow problem. A vanishing in- and out-flow conditions have been imposed at the boundaries of this disk. The gas surrounding the disk is taken to be inviscid, thin, hot and non-rotating. Thus, the flow configuration is similar to the forward facing step problem usually used for test calculations in CFD. The disk here serves as a barrier that forbids the gas from freely falling onto the black hole, and instead, it forms a curved shock front around the cold disk. The purpose of this test is mainly to examine the capability of the hierarchical scenario at employing the semi-explicit method adequately and enables capturing steady solution governed by strong shocks. In solving the HD-equations, an advection scheme of third order spatial accuracy and first order accurate in time has been used. The domain of calculation is sub-divided into 200 strongly-stretched finite volume cells in the radial direction and 60 in horizontal direction. In Fig. 5 the configuration of the steady distributions of the density, temperature and the velocity field are shown. Similar to the calculation in the previous sub-section, the results indicate that the method employed is stable and converges to the sought steady solution even when a CFL-number of order 200 is used. However, the method converges relatively slowly compared to the implicit operator splitting approach, where steady solutions have been obtained after one thousand iterations only.

4.3 Formation and acceleration of proton-dominated jets in active galaxies

To study the mechanisms underlying jet formation around black holes, we have placed initially a classical accretion disk within the first 20 last stable radii, sandwiched by a hot and tenuous corona, and threaded by a large scale magnetic field. The solution procedure run as follows:

1. The HD-equations are solved using the IOS-approach as depicted in Stage I of Fig. 3. The calculations were run to cover the viscous time scale.
2. Using the obtained results from the previous stage as starting conditions, Stage II of the global solution procedure is now employed to run the calculations for an additional viscous time scale. Here, the HD and the MHD equations are solved in a blockwise manner as described in Fig. 3. Stage III was not employed, as Alfvén-waves propagation enhances the time-dependency of the flow even more.
3. The final flow-configuration apparently governed by inflow and outflow plasmas. In general, outflows are gravitationally unbound, and therefore the corresponding Bernoulli number should be positive, whereas negative numbers correspond to gravitationally bound flows that should end their motion inside the black hole. Fig. 6 shows the 2D distribution of the Bernoulli number which obviously show the locations of the gravitationally-bound and unbound flows.

4.4 The spectral energy distribution of the in- and outflow around the supermassive black hole of the giant elliptical galaxy M87

The results obtained in the previous subsection are used to construct the spectral energy distribution. Therefore, the last stage of the hierarchical scenario is now employed in combination with Stage II. Here, the solver of Stage II is activated once every several dozens iterations of the RT-solver.

In Fig. 9 we display the results of several calculations under various conditions. The results displayed in Fig. 7 and 8 are preliminary, as the distributions of the density and temperature used here are artificial, but aimed at testing the convergence of the RT-solver.

5 The combined solution procedure: The hierarchical scenario

In the following we describe the main steps of a possible algorithmic procedure for solving the combined set of MHD and the RT equations (see Stages III and IV of Fig. 3):

1. Compute the RHS_i and the Jacobian $A_i = \partial L_{q_i}/\partial q_i$ of each physical variable $q_i (= \rho, m, n, \dots)$, where L_{q_i} is the equation describing the evolution of variable q_i .
2. For each equation L_{q_i} , compute the coefficient matrices $B_i = \partial L_{q_i}/\partial q_j$, for which $i \neq j$. This procedure applies for advection and diffusive operators only, though not for the source terms.
3. Compute the coefficient matrices corresponding to the source terms only, i.e., $H_i = \partial L_{q_i}/\partial q_j$, for $i = 1, N$ and $j = 1, N$, and $i \neq j$.

The separation of the above-mentioned procedures is essential for enhancing the global efficiency of the hierarchical method. Specifically, the computation of each of the B_i and H_i is optional, depending on the problem in hand. For example, to solve the system of equations corresponding to the hydrodynamical and isothermal flow in 1D efficiently, the numerical algorithm should be capable of calling the relevant routines only. Thus, non-relevant routines can be switched off almost automatically, depending on the problem in hand. In particular, enlarging (reducing) dimensions, incorporating additional (excluding) variable should be algorithmically maintainable.

Taking into account that most astrophysical flows are of multi-scale by nature, we think that the hierarchical solution strategy might be a promising approach. In the following, we describe briefly the basis of this hierarchical scenario applied to set of radiative MHD and the RT equations.

1. The hierarchical approach, or equivalently the multi-stage solution procedure, is based primarily on designing the global solver in such a manner to achieve maximum flexibility. Specifically, the numerical algorithm should be capable of solving the equations sequentially, block-sequential and/or in a fully-coupled manner. Re-ordering and using different pre-conditioning should be maintainable without changing the core of the inverter.
2. As far as vortex-free compressible, viscous and time-dependent flows are concerned, the implicit operator splitting approach (IOS) has been verified to be efficient and robust. IOS is most appropriate for astrophysical fluid simulations, when the sought solutions depend weakly on the initial conditions, but strongly on the boundary conditions. The IOS-method is based on solving the set of equations sequentially as described in Stage I of Fig. 3. The convergence rate of the IOS-method may depend considerably on the order in which the equations are solved, provided the number of global iterations is low.
3. The coupling between the equations can be enhanced gradually. From the cluster of coefficients, we may construct the Jacobians A^{HD} and A^{MHD} , which correspond to the set of HD and MHD equations (see Stage II/Fig. 3). Algorithmically, this procedure is basically a sort of re-ordering and re-organizing of the coefficients, and does not require an extensive programming. As in the previous step, the order in which the equations are solved may affect both its convergence rate and efficiency. Here, a special care should be given to assure that the inclusion of coefficients corresponding to the source terms does not enlarge the band width of A^{HD} and A^{MHD} . Test calculations have shown that careful ordering of the HD-equations may reduce the computational costs devoted for matrix inversion by 75% (HUU1). Furthermore, it has been verified that several equations can still be separated and solved sequentially. Namely, the Poisson equation for modelling self-gravity as well as the angular momentum equation accept partial decoupling from the rest of equations, provided the flow is axisymmetric.

4. Using the solutions obtained in stage II as initial conditions, we may solve the whole set of HD and MHD equations as a single set of coupled equations. The resulting Jacobian is highly sparse, for which pre-conditioned Krylov sub-iterative methods are highly appropriate.
5. By iterating over Stage II and IV, we can be sure that the resulting solution is reasonably close to sought quasi-stationary or steady solutions for the radiative MHD and radiative transfer equations. This is a consequence of:
 - a) The radiative intensity in the high density regions, where the optical thickness is large, is isotropic and coincides with black-body emission. Therefore, the intensity obtained by solving the zero moment of the radiation field is sufficiently accurate in this regime.
 - b) The radiative intensity obtained by solving the RT-equation in optically thin regions may differ considerably from that obtained using the gray approximation. However, radiation in such regions have negligible power and they may hardly affect the dynamics of the flow. Consequently, the following solution method may be proposed:
 - The numerical values of the variables obtained in Stage III are used as initial conditions for calculating the non-gray and time-dependent radiative intensity.
 - The mean-value of the frequency-dependent intensity is computed and subsequently used as initial condition for the radiative MHD equations.
 - To avoid extensive computational costs, it is suggested to solve for I_ν every 10, or 20 time-steps. However, since the radiative time-scale is extremely short compared to the hydrodynamical time scale, it is much more reasonable to solve for the time-independent intensity.

6 Summary

In this paper we have presented the hierarchical scenario for solving the set of radiative MHD equations and the 5D axi-symmetric radiative transfer equation.

The main features of this scenario are as follows:

1. The global efficiency can be enhanced, depending on the optimal architecture of the global solver. Specifically, the algorithmic structure should be sufficiently flexible, so that scalar or set of equations in arbitrary dimensions, different accuracies and using the appropriate pre-conditionings can be solved with a reasonable efficiency.
2. Robustness is monitored through employing a variety of solution procedures. Depending on the particular features of the problem considered,

several stages of implicitness may be used, depending on the number of coefficients used for constructing the coefficient matrix. In particular, starting with a purely explicit time-stepping scheme, the algorithm should be capable of modifying the scheme into a fully implicit method dynamically.

3. For implicit calculations, the hierarchical algorithm relies on using a variety of preconditioning for accelerating convergence. For example, for modelling weakly incompressible flows, it has been verified that the "Approximate Factorization Method" as pre-conditioning yields a larger convergence rate than the "Alternating Directional Implicit" or the "Line Gauss-Seidel" methods. However, the latter preconditionings provide faster convergence if the flow is compressible and advection-dominated. Therefore, depending on the problem in hand, the algorithm should be capable of employing the appropriate preconditioning at least in an explicit-adaptive manner.
4. The hierarchical algorithm is capable of solving the angle-averaged time-dependent radiation transfer equation, taking into account the Kompaneets operator for modelling up-scattering of soft photons by hot electrons in magnetized plasmas.

We note, however, that the assumption of isotropic radiative intensity may break down if the flow is relativistic and contains regions of significantly different optical depths. Therefore, in the near future we intend to modify the RT-solver to enable modelling the motions of ultra-relativistic plasmas in the vicinities Kerr and Schwarzschild black holes.

5. The algorithm includes a procedure that allows solving the zero-moment MHD equations partially/loosely coupled with the radiation transfer equations. The latter coupling can be significantly enhanced through parallelization on powerful machines.

Finally, we have shown that the hierarchical algorithm presented here can be applied to study the mechanisms underlying the formation, launching and acceleration of jets in AGNs and quasars, though serious numerical and physical modifications are still required.

References

- [BA91] Balbus, S., Hawley, J., 1991, "A powerful local shear instability in weakly magnetized disks. I - Linear analysis. II - Nonlinear evolution", *ApJ*, **376**, 214
- [BW78] Beam, R.M., Warming, R.F., 1978, "An implicit factorized scheme for compressible Navier-Stokes equations", *AIAA*, **16**, 393
- [BR01] Brandt, A., 2001, "Textbook Multi-grids", in *Multigrid*, ed.: Trottenberg, U., Oosterlee, C., Schüller, A., Acad. Press, London
- [DO98] Dongarra, I.S., Duff, D.C., Sorensen, H.A., van der Vorst, 1998, "Num. Linear Alg. for High-Performance Computers", *SIAM J. Scient. Comput.*, **20**, 94

- [FE72] Felten, J.E., & Rees, M.J., 1972, “Transfer effects on lines and continuum in optically thick sources”, *A&A*, **21**, 139
- [FL88] Fletcher, C.A.J., 1988, ‘Computational Techniques for Fluid Dynamics’, Vol, I and II, Springer-Verlag
- [FO00] Font, J. A. 2000, “Numerical Hydrodynamics in General Relativity”, *Living Rev. Relativity*, **3**, 2
- [FR00] Fryxell, B., Olson, K., Ricker, P., et al., 2000, “FLASH: An Adaptive Mesh Hydrodynamics Code for Modeling Astrophysical Thermonuclear Flashes”, *ApJS*, **131**, 273
- [GA03] Gammie, C.F., McKinney, J.C., Tóth, G., 2003, “HARM: A Numerical Scheme for General Relativistic Magnetohydrodynamics”, *ApJ*, **589**, 444
- [HI90] Hirsch, C., 1990, ‘Num. Computation of Internal and External Flows’, Vol, I, and II, John Wiley & Sons, New York
- [HUJ0] Hujeirat, A., Papaloizou, J.C.P., 1998, “Shock formation in accretion columns - a 2D radiative MHD approach”, *A&A*, **340**, 593
- [HUJ1] Hujeirat, A., Rannacher, R., 2001, “On the efficiency and robustness of implicit methods in computational astrophysics”, *NewAR*, **45**, 425
- [HUJ2] Hujeirat, A., Camenzind, M., Livio, M., 2002, “Ion-dominated plasma and the origin of jets in quasars”, *A&A*, **394**, L9
- [HUJ3] Hujeirat, A., Camenzind, M., Burkert, A., 2002b, “Comptonization and synchrotron emission in 2D accretion flows. I. A new numerical solver for the Kompaneets equation”, *A&A*, **386**, 757
- [HUJ5] Hujeirat, A., Livio, M., Camenzind, M., Burkert, A., 2003, “A model for the jet-disk connection in BH accreting systems”, *A&A*, **408**, 415
- [HUJ6] Hujeirat, A., Blandford, R.D., 2004, “A model for electromagnetic extraction of rotational energy and formation of accretion-powered jets in radio galaxies”, *A&A*, **416**, 423
- [HUJ8] Hujeirat, A., 2004, “A method for enhancing the stability and robustness of explicit schemes in CFD”, in press, *New Astronomy Reviews*.
- [KA76] Katz, J.A., 1976, “Nonrelativistic Compton scattering and models of quasars”, *ApJ*, **206**, 910
- [IL72] Ilyarinov, A.F., & Sunyaev, R.A., 1972, “Compton scattering by thermal electrons in X-ray sources ” *Soviet Astr. -AJ*, **16**, 45
- [KL89] Kley, W., 1989, “Radiation hydrodynamics of the boundary layer in accretion disks. I - Numerical methods”, *A&A*, **208**, 98
- [KO99] Koide, S., Shibata, K., & Kudoh, T. 1999, “Relativistic Jet Formation from Black Hole Magnetized Accretion Disks: Method, Tests, and Applications of a General Relativistic Magnetohydrodynamic Numerical Code”, *ApJ*, **522**, 727

- [KO02] Koide, S., Shibata, K., Kudoh, T., & Meier, D. L. 2002, “Extraction of Black Hole Rotational Energy by a Magnetic Field and the Formation of Relativistic Jets”, *Science*, **195**, 1688
- [KO99] Komissarov, S. S. 1999, “A Godunov-type scheme for relativistic magnetohydrodynamics”, *MNRAS*, **303**, 343
- [LE81] Levermore, C.D., & Pomraning, G.C., 1981, “A flux-limited diffusion theory”, *ApJ*, **248**, 321
- [MA96] Mahadevan, R., & Narayan, R., Yi, I., 1996, “Harmony of electrons: Cyclotron and Synchrotron emission by thermal electrons in magnetic fields”, *ApJ*, **465**, 327
- [MA85] MacCormack, R.W., 1985, “Current status of numerical solutions of Navier-Stokes equations”, AIAA, Paper 81-0110
- [MA99] Martí, J.M., Müller, E., 1999, “Numerical hydrodynamics in special relativity”, *Living Rev. Relativity*, **2**, 3
- [ME01] Meier, D.L., Koide, S., & Uchida, Y. 2001, “Magnetohydrodynamic Production of Relativistic Jets”, *Science*, **291**, 84
- [ME03] Meier, D., 2003, “The theory and simulation of relativistic jet formation: towards a unified model for micro- and macroquasars”, *NewAR*, **47**, 667
- [MI86] Mihalas, D., Mihalas, B.W., 1984, “Foundations of radiation hydrodynamics”, Oxford University Press, NY, (MM)
- [OU97] Ouyed, R., Pudritz, R., 1997, “Numerical simulation of astrophysical jets from Keplerian disks. II. episodic outflows”, *ApJ*, **484**, 794
- [PA80] Payne, D.G., 1980, “Time-dependent Comptonization - X-ray reverberations”, *ApJ*, **237**, 951
- [RY79] Rybicki, G.B., & Lightman, A.P., 1979, *Radiation processes*, Wiley-Interscience Publication
- [SA00] Saad, Y., van der Vorst, 2000, “Iterative solution of linear systems in the 20-th century”, *J. of Comp. and Appl. Math.*, **123**, 1
- [SH76] Shapiro, S.L., Lightman A.P., & Eardley, D.M., “A two-temperature accretion disk model for Cygnus X-1 structure and spectrum”, 1976, *ApJ*, **204**, 187
- [ST92] Stone, J.M., & Norman, M., 1992, “ZEUS-2D: A radiation magnetohydrodynamics code for astrophysical flows in two space dimensions. I - The hydrodynamic algorithms and tests.”, *ApJS*, **80**, 791
- [TO98] Tóth, Keppens, R., Botchev, M.A., 1998, “Implicit and semi-implicit schemes in the Versatile Advection Code: numerical tests”, *A&A*, **332**, 1159
- [TR01] Trottenberg, U., 2001, in *Multigrid*, ed.: Trottenberg, U., Oosterlee, C., Schüller, A., Acad. Press, London
- [UC99] Uchida, Y., Nakamura, M., Hirose, S., Uemura, S., “Magnetodynamic formation of jets in accretion process of magnetized mass onto the central gravitator”, *Ap&SS*, **264**, 195

[VI03] De Villiers, J.-P., & Hawley, J.F., 2003, “A Numerical Method for General Relativistic Magnetohydrodynamics”, *ApJ*, **589**, 458

[ZI98] Ziegler, U., 1998, “NIRVANA+: An adaptive mesh refinement code for gas dynamics and MHD”, *Comp. Phys. Comm.*, **109**, 142

This figure "Fig5.jpg" is available in "jpg" format from:

<http://arxiv.org/ps/math-ph/0410055v1>

This figure "Fig6.jpg" is available in "jpg" format from:

<http://arxiv.org/ps/math-ph/0410055v1>

This figure "Fig9a.jpg" is available in "jpg" format from:

<http://arxiv.org/ps/math-ph/0410055v1>